





RESEARCH ARTICLE

Increased uptake of the P2X7 receptor radiotracer ^{18}F -JNJ-64413739 in the brain and peripheral organs according to the severity of status epilepticus in male mice

James Morgan^{1,2}  | Oscar Moreno³ | Mariana Alves¹ | Zuriñe Baz³ | Aida Menéndez Méndez¹ | Hanna Leister⁴ | Ciara Melia¹ | Jonathon Smith^{1,5} | Alexander Visekruna⁴ | Annette Nicke⁶ | Anindya Bhattacharya⁷ | Marc Ceusters^{8,9} | David C. Henshall^{1,5}  | Vanessa Gómez-Vallejo³ | Jordi Llop³  | Tobias Engel^{1,5} 

¹Department of Physiology and Medical Physics, Royal College of Surgeons in Ireland, University of Medicine and Health Sciences, Dublin, Ireland

²Division of Developmental Biology and Medicine, School of Medical Sciences, Faculty of Biology, Medicine, and Health, University of Manchester, Manchester, UK

³CIC biomaGUNE, Basque Research and Technology Alliance (BRTA), San Sebastian, Spain

⁴Institute for Medical Microbiology and Hygiene, Philipps University, Marburg, Germany

⁵FutureNeuro, Science Foundation Ireland (SFI) Research Centre for Chronic and Rare Neurological Diseases, Royal College of Surgeons in Ireland, University of Medicine and Health Sciences, Dublin, Ireland

⁶Walther Straub Institute of Pharmacology and Toxicology, Ludwig Maximilian University of Munich, Munich, Germany

⁷Neuroimmunology Discover, Neuroscience, Janssen Research and Development, San Diego, California, USA

⁸Neuroscience Therapeutic Area, Janssen Research and Development, Janssen Pharmaceutica, Beerse, Belgium

⁹Marc Ceusters Company, Beerse, Belgium

Correspondence

Tobias Engel, Department of Physiology and Medical Physics, RCSI, University of Medicine and Health Sciences, D02 YN77, Dublin, Ireland.
Email: tengel@rcsi.ie

Funding information

H2020 Marie Skłodowska-Curie Actions, Grant/Award Number: 766124 and 884956; Irish Research Council for Science, Engineering and Technology, Grant/Award Number: GOIPD/2020/865; MCIN/AEI/10.13039/501100011033, Grant/Award Number: MDM-2017-0720 and PID2020-117656RB-I00; Science Foundation Ireland, Grant/Award Number: 16/RC/3948 and 17/

Abstract

Objective: The P2X7 receptor (P2X7R) is an important contributor to neuroinflammation, responding to extracellularly released adenosine triphosphate. Expression of the P2X7R is increased in the brain in experimental and human epilepsy, and genetic or pharmacologic targeting of the receptor can reduce seizure frequency and severity in preclinical models. Experimentally induced seizures also increase levels of the P2X7R in blood. Here, we tested ^{18}F -JNJ-64413739, a positron emission tomography (PET) P2X7R antagonist, as a potential noninvasive biomarker of seizure-damage and epileptogenesis.

Methods: Status epilepticus was induced via an intra-amygdala microinjection of kainic acid. Static PET studies (30 min duration, initiated 30 min after tracer administration) were conducted 48 h after status epilepticus via an intravenous injection of ^{18}F -JNJ-64413739. PET images were coregistered with a brain magnetic

Jordi Llop and Tobias Engel contributed equally to this work.

This is an open access article under the terms of the [Creative Commons Attribution-NonCommercial-NoDerivs](https://creativecommons.org/licenses/by-nc-nd/4.0/) License, which permits use and distribution in any medium, provided the original work is properly cited, the use is non-commercial and no modifications or adaptations are made.

© 2022 The Authors. *Epilepsia* published by Wiley Periodicals LLC on behalf of International League Against Epilepsy.

CDA/4708; European Regional Development Fund; European Union; Horizon 2020; Research Foundation

resonance imaging atlas, tracer uptake was determined in the different brain regions and peripheral organs, and values were correlated to seizure severity during status epilepticus. ^{18}F -JNJ-64413739 was also applied to ex vivo human brain slices obtained following surgical resection for intractable temporal lobe epilepsy.

Results: P2X7R radiotracer uptake correlated strongly with seizure severity during status epilepticus in brain structures including the cerebellum and ipsi- and contralateral cortex, hippocampus, striatum, and thalamus. In addition, a correlation between radiotracer uptake and seizure severity was also evident in peripheral organs such as the heart and the liver. Finally, P2X7R radiotracer uptake was found elevated in brain sections from patients with temporal lobe epilepsy when compared to control.

Significance: Taken together, our data suggest that P2X7R-based PET imaging may help to identify seizure-induced neuropathology and temporal lobe epilepsy patients with increased P2X7R levels possibly benefitting from P2X7R-based treatments.

KEYWORDS

diagnosis, epilepsy, P2X7 receptor, positron emission tomography, status epilepticus

1 | INTRODUCTION

Major challenges of epilepsy treatment include drug-refractoriness and a correct diagnosis.¹ Epileptogenesis, caused by a precipitating injury to the brain (e.g., traumatic brain injury [TBI], status epilepticus [SE]), is the process of turning a healthy brain into a brain experiencing epileptic seizures.² To date, there are no diagnostic tools to identify patients who will develop epilepsy, further complicating epilepsy management.

Adenosine triphosphate (ATP) acts as a cotransmitter to regulate brain network excitability via the activation of purinergic P2 receptors,³ including the ligand-gated cationic P2X receptors.⁴ Among these, the P2X7 receptor (P2X7R) has attracted attention as potential drug target and biomarker for epilepsy.^{3,5} The relatively low affinity for ATP ($\text{EC}_{50} \geq 100 \mu\text{mol}\cdot\text{L}^{-1}$) probably restricts P2X7R activation to conditions of pathological ATP release,⁶ suggesting fewer side effects during P2X7R-based treatments. P2X7R has slow desensitization dynamics and an ability to permeabilize the cell membrane to molecules up to 900 Da and is a key driver of inflammation.^{3,7,8} P2X7R is, however, also involved in numerous other pathways pertinent to epileptogenesis including synaptic plasticity, neurogenesis, and the regulation of neurotransmitter release.^{9,10} Increased P2X7R expression has been extensively documented in experimental and human epilepsy in the hippocampus and neocortex.^{11–16} Targeting of P2X7R modulates severity of SE in mice^{13–15,17,18} and suppresses seizures in models of drug-resistant epilepsy.^{16,19} More

Key Points

- P2X7R radiotracer uptake levels in the brain and peripheral organs correlate with severity of status epilepticus
- P2X7R radiotracer uptake is increased in brain sections from resected tissue of patients with temporal lobe epilepsy
- P2X7R PET imaging may represent a new diagnostic tool for patients according to seizure-induced neuropathology and epilepsy

recent data show that increased P2X7R expression leads to unresponsiveness to antiseizure drugs (ASDs).²⁰

Positron emission tomography (PET) is a powerful, noninvasive tool for the identification of disease-specific biomarkers. In epilepsy, PET is primarily used to image glucose metabolism by using the radiotracer 2- ^{18}F fluoro-2-deoxy-D-glucose (^{18}F fluorodeoxyglucose or ^{18}F FDG), particularly in temporal lobe epilepsy (TLE), the most common and drug-refractory form of epilepsy in adults.¹ In recent years, radiotracers have, however, advanced beyond the identification of altered glucose metabolism, and ligand-specific radiotracers are currently being investigated. In particular, radioligands recognizing inflammatory molecules such as the translocator protein (TSPO), a marker of activated glia, have shown promising results as prognostic markers of drug-refractory TLE.^{21–24}

Although P2X7R radiotracer uptake has successfully been detected in the brain of rodents and humans,^{25,26} whether altered P2X7R expression following SE can be detected via PET and whether this signal reflects underlying pathology relevant to epilepsy remain unknown.

Using a mouse model of SE leading to drug-resistant focal epilepsy,²⁷ we show acute elevation in signal from the P2X7R-specific radiotracer ¹⁸F-JNJ-64413739 according to severity of SE in the brain and peripheral organs. P2X7R radioligand uptake was also increased in resected brain tissue of TLE patients. Together, our findings suggest that PET imaging of P2X7R may help to identify patients with increased P2X7R expression and, hence, in need of P2X7R-based treatments.

2 | MATERIALS AND METHODS

Reagents were purchased from Sigma-Aldrich if not stated otherwise. See [Table S3](#) for details on antibodies.

2.1 | Animals

Animal experimentation ([Table S1](#)) was conducted in accordance with the European Council Directive 2010/63/EU at the facilities of CIC biomaGUNE (San Sebastián, Spain) and the Royal College of Surgeons in Ireland (RCSI) and approved by the Ethical Committee at CIC biomaGUNE and Diputación Foral de Guipúzcoa (PRO-AE-SS-123), the Research Ethics Committee at RCSI (REC 1322), and the Health Products Regulatory Authority (AE19127/P038). Here, we used 8–10-week-old male C57/Bl6 OlaHsd mice, P2X7R knockout (*P2rx7*^{-/-}) mice (6NTac;B6N-P2rx7tm1d [EUCOMM]Wtsi/Ieg), and FVB/NJ BAC mice (FVB/N-Tg[RP24-114E20-P2X7/StrepHisEGFP]) that express the enhanced green fluorescent protein (EGFP) immediately upstream of a *P2rx7* BAC clone (P2X7R-EGFP).²⁸ Animals were housed in a controlled biomedical facility on a 12-h light/dark cycle at 22±1°C and humidity of 40%–60% with food and water provided ad libitum.

2.2 | SE mouse model

Fully anesthetized mice were placed in a stereotaxic frame, and a midline scalp incision was performed to expose the skull. A guide cannula for intra-amygdala kainic acid (IACA; coordinates from bregma: anteroposterior = −.94 mm, lateral = −2.85 mm) was fixed in place with dental cement. SE was induced in awake, hand-restrained mice, by a microinjection (3.75 mm below brain surface) of .3 µg kainic acid (KA; C57/Bl6) or .2 µg KA

(FVB/NJ) in .2 µl phosphate-buffered saline (PBS) into the right basolateral amygdala.²⁰ Vehicle-injected control animals received .2 µl intra-amygdala PBS. Lorazepam (6 mg/kg ip; Wyetch) was delivered 40 min post-IACA/vehicle. A subset of mice, not used for PET, were fitted with cortical electrodes fixed with dental cement, one on top of each hippocampus and the reference electrode on top of the frontal cortex. Electroencephalogram (EEG) was recorded using an Xltek recording system (Optima Medical) starting 10 min before IACA.

2.3 | Analysis of seizure severity during SE

Behavioral seizures were scored according to a modified Racine Scale²⁹: score = 1, immobility and freezing; score = 2, forelimb and/or tail extension, rigid posture; score = 3, repetitive movements, head bobbing; score = 4, rearing and falling; score = 5, continuous rearing and falling; score = 6, severe tonic-clonic seizures. Mice were scored every 5 min for 40 min after KA injection. All mice used for our studies reached at least score = 3 on the Racine scale. The highest score attained during each 5-min period was recorded by an observer unaware of treatment. To analyze EEG frequency and amplitude signal, EEG data were uploaded onto Labchart7 software (AD Instruments) and analyzed.³⁰ EEG total power (µV²) is a function of EEG amplitude over time and was analyzed by integrating frequency bands from 0 to 100 Hz and the amplitude domain filtered from 0 to 50 mV.³⁰

2.4 | Human brain tissue

Resected hippocampal tissue from patients with refractory TLE ($n = 14$, mean age = 42.14±3.3 years, 71.5% male) was provided by Ryder Gwinn (Swedish Medical Center).³¹ Informed consent was obtained for all patients ([Supplementary Table S2](#)). Control hippocampi ($n = 3$, mean age 39.25±4.5, 75% male), with no history of neurological disease, were obtained from the University of Maryland Brain and Tissue Bank and from the UK Brain Bank.

2.5 | Western blotting

Western blotting was carried out as before using 30–50 µg of protein per sample loaded onto an acrylamide gel and separated by sodium dodecyl sulphate–polyacrylamide gel electrophoresis.²⁰ Following electrophoresis, proteins were transferred to a nitrocellulose membrane (GE

Healthcare) and immunoblotted with primary antibodies. Membranes were incubated with horseradish peroxidase-conjugated goat antirabbit or antimouse secondary antibodies (1:5000). Protein bands were visualized using the Fujifilm LAS-4000 system with chemiluminescence (Immobilon Western HRP Substrate, Merck Millipore) followed by analysis using Alpha-EaseFC4.0 software. Spot dense option was used to evaluate the optical density of each protein band. Protein quantity was normalized to loading control β -actin or glyceraldehyde-3-phosphate dehydrogenase.

2.6 | Immunofluorescence

Mice were transcardially perfused with PBS followed by 4% paraformaldehyde (PFA), and brains were removed. Following 24 h of postfixation in 4% PFA at 4°C, brains were transferred to PBS and immersed into 4% agarose. Fifty-micrometer sagittal sections were cut using the VT1000S vibratome and stored at -20°C in glycol. Tissue sections were incubated with .1% Triton/PBS, followed by 1 mol·L⁻¹ glycine and with 1% bovine serum albumin (BSA)-PBS. Sections were then incubated with primary antibodies overnight. After washing in PBS, tissue was incubated with fluorescent secondary antibodies, followed by a short incubation with 4,6-diamidino-2-phenylindole (DAPI; 1:500). FluorSave (Millipore) was used to mount the tissue. Confocal images were taken with a Zeiss 710 LSM NLO confocal microscope equipped with four laser lines (405, 488, 561, and 653 nm) using a $\times 40$ oil immersion objective and ZEN 2010B SP1 software.

For immunofluorescence using P2X7R nanobodies,²⁰ tissue sections were washed in .1% Triton X-100 for 7 min and blocked with .05% saponin/3% BSA/15 mmol·L⁻¹ NH₄Cl/PBS for 20 min. Antibodies against P2X7R and green fluorescent protein (GFP) were incubated overnight at 4°C in blocking buffer without saponin. After three washes with PBS, sections were incubated for 2 h at room temperature with secondary antibodies, washed three times with PBS, shortly stained with DAPI (1 mg/L, Carl Roth), washed with water, and mounted (PermaFluor, Thermo Fisher) for confocal microscopy.

2.7 | Radiochemistry

¹⁸F-JNJ-64413739 synthesis was performed using a TRACERlab FX_{FN} synthesis module (GE Healthcare) following a previously described method with minor modifications.³² [¹⁸F]F⁻ was generated in a Cyclone 18/9 cyclotron (IBA) by proton irradiation of ¹⁸O-enriched

water via the ¹⁸O(p,n)¹⁸F nuclear reaction, and trapped on a preconditioned Sep-Pak Accell Plus QMA Light cartridge (Waters). The trapped [¹⁸F]F⁻ was eluted with a solution of Kryptofix K_{2.2.2}/K₂CO₃ in a mixture of acetonitrile/water (2:1, 1.5 ml). After complete elimination of the solvent by azeotropic evaporation, a solution containing the precursor (JNJ-64410047, 4 mg) in dimethylsulfoxide (.7 ml) was added, and the mixture was heated at 120°C for 15 min. After cooling to room temperature, the mixture was purified by high-performance liquid chromatography (HPLC) using a Phenomenex Luna C18 (250 mm) column as the stationary phase and water (.1% trifluoroacetic acid [TFA])/acetonitrile (65/35, vol/vol) as the mobile phase (flow rate = 4 ml/min). The desired fraction (retention time = 18.0 min) was collected, diluted with a sodium ascorbate solution, and reformulated using a C-18 light cartridge (Sep-Pak Plus, Waters). The resulting ethanol solution (1 ml) was diluted with 9 ml of sodium ascorbate solution to yield an injectable solution of the radiotracer. Chemical and radiochemical purity were determined by radio-HPLC, and identity of the desired tracer was confirmed by coelution with reference standard. An Agilent Eclipse XBD-C18 (4.6 \times 150 mm, 5 μ m) was used as the stationary phase and water (.1% TFA)/acetonitrile (70/30, vol/vol) as the mobile phase at a flow rate of 1 ml/min (retention time = 12.5 min). Decay-corrected radiochemical yield was 6.9 \pm .5% (total synthesis time: 90 min). Radiochemical purity was >99%, and molar activity values were within the range of 25–95 GBq/ μ mol at the end of the synthesis.

2.8 | In vitro PET studies

Animals were transcardially perfused with saline, and brains were harvested, fast-frozen at -80°C, and cut into 25 μ m slices. Brain slices were preincubated with PBS (10 mmol·L⁻¹, pH = 7.4) for 10 min at 25°C. Subsequently, samples were incubated (30 min, 25°C) with ¹⁸F-JNJ-64413739 (ca. 74 MBq) at two different concentrations (10 nmol·L⁻¹ and 100 nmol·L⁻¹, the latter to block specific binding). After incubation, brain slices were rinsed twice with cold PBS (10 mmol·L⁻¹, pH = 7.4) and once with ultrapure cold water, dried at 50°C, and then measured using a β -cube microsystem (Molecubes) for 1 h. Images were reconstructed using the OSEM-3D iterative algorithm, regions of interest were defined in the whole brain slices, and the surface concentration of radioactivity for each slice was determined. The same procedure was applied to frozen brain sections from TLE patients. For control subjects, and before incubation with ¹⁸F-JNJ-64413739, paraffin-embedded slices were rehydrated by incubation in the following consecutive solutions at room temperature: 100% xylene (10 min), 100% ethanol (3 min),

95% ethanol (3 min), 70% ethanol (3 min), 50% ethanol (3 min), and ultrapure water (10 min).

2.9 | In vivo PET-computerized tomographic studies

PET-computerized tomographic (CT) imaging was conducted using β - and X-cube microsystems (Molecubes). Radiotracer (2.5–7.4 MBq, 100 μ l) was injected intravenously via one of the lateral tail veins in anesthetized mice. Thirty minutes after radiotracer administration, animals were positioned in a PET scanner and static 30-min PET images were acquired in one bed position, with animals centered in the middle of the field of view. Scan times were corrected for the delay in PET experiment initialization. CT scans were acquired immediately after each PET acquisition. PET images were reconstructed by OSEM-3D iterative algorithm. Images were analyzed using π -MOD image analysis software. Volumes of interest were delineated in different brain regions (whole brain and ipsi- and contralateral cerebral cortex, hippocampus, striatum, cerebellum, thalamus, and amygdala) using the M. Mirrione-T2 magnetic resonance imaging template. Uptake in the different regions/peripheral organs (heart, liver, lung, kidney) was determined as a percentage of injected dose per cubic centimeter of tissue.

2.10 | Statistical analysis

Statistical analysis was carried out using Prism 5 (GraphPad) and STATVIEW software (SAS Institute). Data are presented as mean \pm SD. One-way analysis of variance (ANOVA) parametric statistics with post hoc Fisher protected least significant difference test was used to determine statistical differences between three or more groups. Unpaired Student *t* test was used for two-group comparisons. Two-way ANOVA was used for measures between groups with two factors. Correlations between variables were assessed using Spearman rank correlation coefficient. Significance was accepted at $p < .05$.

3 | RESULTS

3.1 | P2X7R radiotracer ^{18}F -JNJ-64413739 uptake in brain tissue correlates with severity of SE

The P2X7R radiotracer ^{18}F -JNJ-64413739 has been shown to bind to P2X7R in several species including mice and humans.^{25,32,33} To further confirm its specificity for the murine P2X7R, P2X7R radioligand uptake was measured

in ex vivo assays using brain slices from control wild-type (wt) mice and wt and $P2X7^{-/-}$ mice subjected to SE 48 h after intra-amygdala treatments (KA/vehicle). P2X7R radioligand uptake was decreased in wt mice when incubated with ^{18}F -JNJ-64413739 in the presence of nonradioactive JNJ-64413739, confirming the specific binding of the radiotracer. Contrarily, no difference in uptake was observed for brain slices from $P2X7^{-/-}$ mice post-SE under blocking conditions (Figure 1A,B). Of note, although P2X7R tracer binding was slightly higher in wt mice subjected to SE when compared to wt control mice (Figure 1A,B), this was not statistically significant. To establish the optimal protocol to detect ^{18}F -JNJ-64413739 in the brain in vivo, P2X7R radiotracers were injected 48 h after SE via the tail vein in vehicle-treated control mice and mice subjected to SE, and dynamic images (60 min duration) were acquired immediately after tracer administration to obtain time-activity curves in the brain. The results clearly showed a plateau at $t > 30$ min for both groups (Figure 1C).

To test whether SE leads to changes in P2X7R radiotracer uptake in vivo, ^{18}F -JNJ-64413739 uptake was analyzed in wt mice (SE and control) 48 h post-IACA (Figure 2A), a seizure-free latent period in the model.²⁷ Full body images showed highest tracer uptake in peripheral organs such as the liver and kidneys, with significant accumulation also in the bladder (Figure 2B). In vehicle-injected control mice and mice subjected to SE, P2X7R radiotracer uptake was similar across different brain regions with the highest levels detected in the cerebellum (Figure 2C, Figure S1A), as reported previously.³⁴ Of note, P2X7R radioligand uptake was similar between naïve and vehicle-injected wt control mice (Figure S2). We then compared P2X7R tracer binding between control mice and mice subjected to SE. This revealed similar uptake of ^{18}F -JNJ-64413739 when analyzing the whole brain and different brain regions separately including the ipsi- and contralateral cortex, hippocampus, thalamus, striatum, cerebellum, and amygdala (Figure 2D, Figure S3, Table S4). To determine whether P2X7R radiotracer uptake changes according to severity of SE, mice subjected to SE were separated into two groups: (1) mice that experienced a less severe SE (mild SE, Racine score ≤ 3.5) and (2) mice that experienced a more severe SE (severe SE, Racine score > 3.5). Of note, experiments using a separate set of mice showed that seizure-induced behavior changes during SE correlated strongly with changes on the EEG (Figure S4). This showed that mice that experienced a more severe SE also showed higher P2X7R radiotracer uptake (~15%–20%) when compared to mice with milder SE. This increase was similar for all brain regions analyzed (Figure 2E, Table S4). A strong correlation could be observed between seizure severity and P2X7R

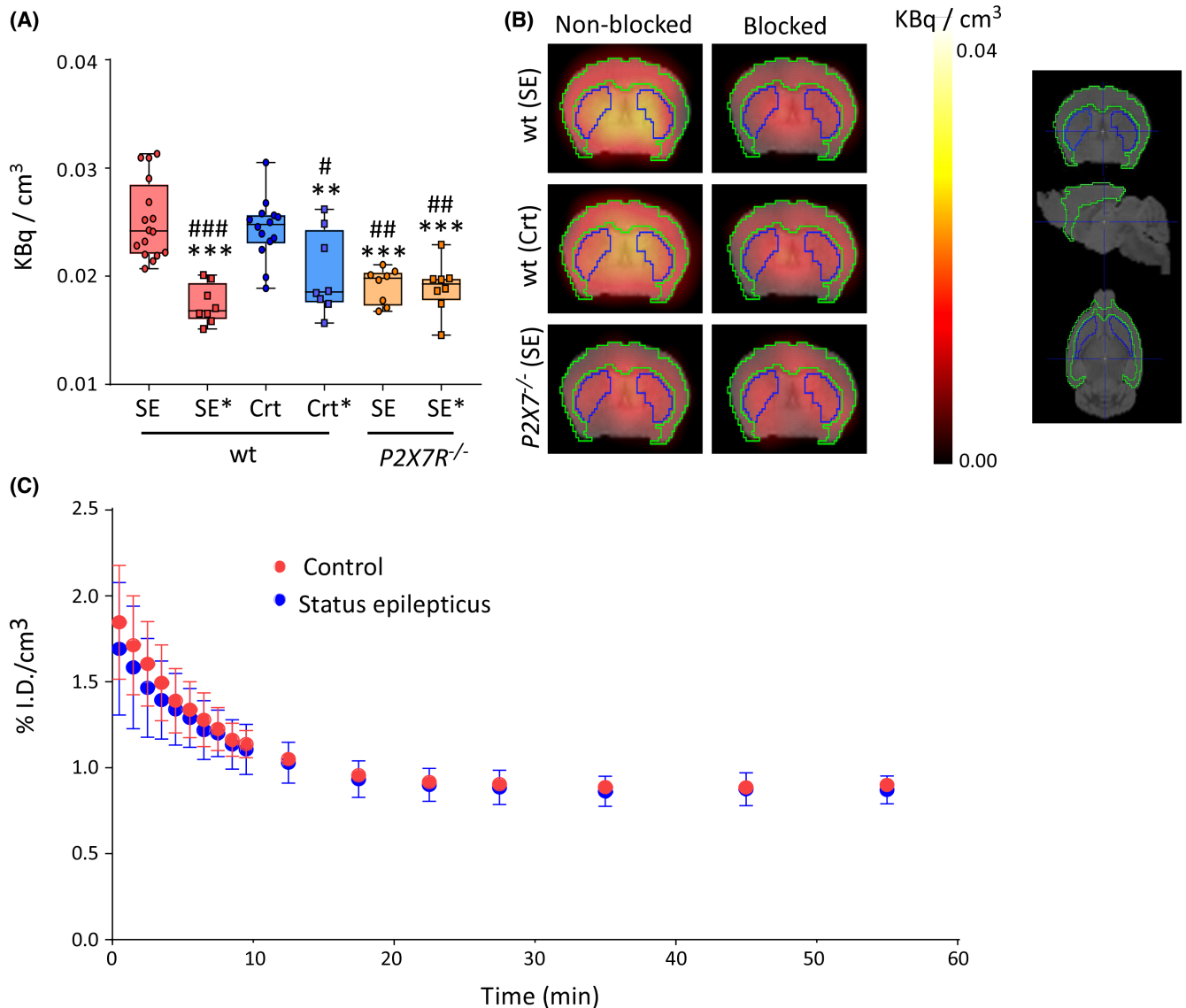
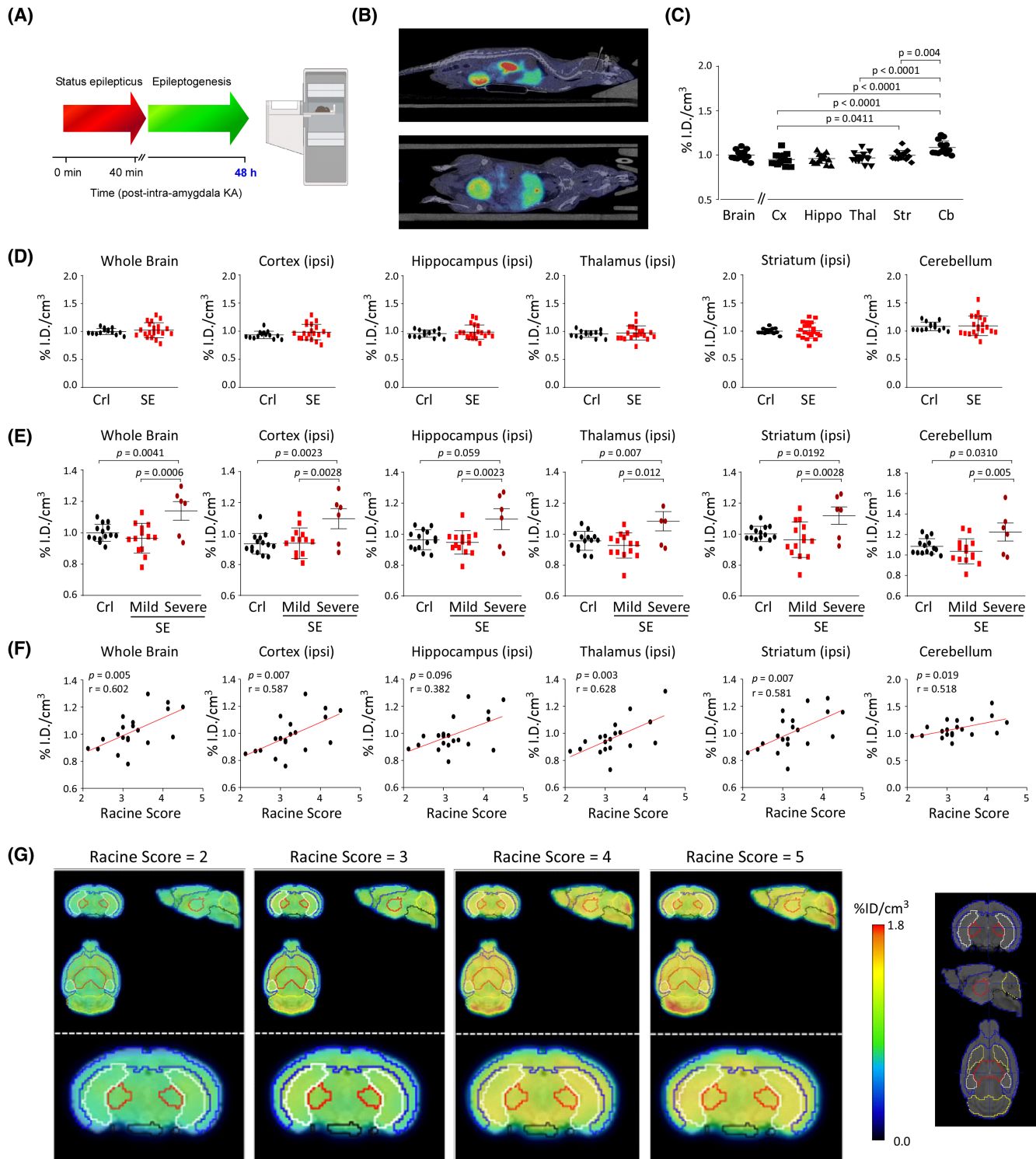


FIGURE 1 Specificity of P2X7 receptor (P2X7R) radiotracer ^{18}F -JNJ-64413739 in brain tissue. (A) Graphs and (B) representative images showing higher uptake of P2X7R radiotracer ^{18}F -JNJ-64413739 measured ex vivo in brain slices from control wild-type (wt) mice and wt mice subjected to status epilepticus (SE) when compared to $P2X7R^{-/-}$ mice subjected to SE 48 h after intra-amygdala injections of kainic acid or vehicle. Inhibition of specific binding was assayed by incubation with ^{18}F -JNJ-64413739 in the presence of nonradioactive JNJ-64413739 ($n = 16$ brain slices from wt post-SE, 14 brain slices from wt control [Crt], and eight brain slices from $P2X7R^{-/-}$ mice; each treatment group represents three independent animals; two-way analysis of variance with multiple comparison; * $p < .05$, ** $p < .01$ and *** $p < .001$ represent differences vs. SE; # $p < .05$, ## $p < .01$ and ### $p < .001$ represent differences vs. Crt; adjusted p -values: SE vs. $P2X7R^{-/-}$: .0002; SE vs. SE*: <.0001; SE vs. Crt*: .0038; SE vs. $P2X7R^{-/-}$ *: .0001; Crt vs. $P2X7R^{-/-}$: .0023; Crt vs. SE*: <.0001; Crt vs. Crt*: .0287; Crt vs. $P2X7R^{-/-}$ *: .0016). (C) Graph showing concentration of radioactivity in the brain, as determined by PET imaging, at different times after administration of ^{18}F -JNJ-64413739 to control wt mice and wt mice subjected to SE ($n = 3$ per group, results expressed as percentage of injected dose per cubic centimeter of tissue [%I.D./cm³], mean \pm SD).

radioligand uptake for all brain regions analyzed, further confirming the strong correlation between seizure severity during SE and P2X7R expression in the brain (Figure 2F,G and Table S5).

To confirm our results via P2X7R PET imaging, we analyzed P2X7R expression in the ipsilateral hippocampus 48 h post-IACA via Western blot in a separate set of mice.

We also analyzed the expression of the P2X4R and the inflammation markers glial fibrillary acidic protein (GFAP; astrocytes) and Iba-1 (microglia). Whereas hippocampal GFAP expression was significantly increased post-SE, P2X7R and Iba-1 showed only a slight increase. Although shown to be increased after intraperitoneal KA-induced SE,³⁵ no change was observed for P2X4R expression



(Figure S5A). Importantly, P2X7R expression showed a similar correlation to seizure severity during SE, confirming our previous observations (Figure S5B). No significant correlation was observed between severity of SE and P2X4R, GFAP, and Iba-1 expression (Figure S5B). Double immunostaining of brain slices from control-treated P2X7R-EGFP mice and P2X7R-EGFP mice subjected to SE

using antibodies against P2X7R and GFP showed a mainly glial expression of P2X7R post-SE in the CA3, a hippocampal subfield particularly affected by seizure-induced neurodegeneration in the model (Figure S5C).^{28,36} The mainly glial expression of P2X7Rs post-SE was further confirmed by using the cell type-specific markers Iba-1 (microglia) and Olig-2 (oligodendrocytes; Figure S5D).

FIGURE 2 P2X7 receptor (P2X7R) radiotracer uptake levels change in the brain in vivo according to seizure severity during status epilepticus (SE). (A) Schematic of experimental design. Positron emission tomographic (PET) imaging was carried out during the seizure-free latent period 48 h after intra-amygdala kainic acid (KA). (B) Representative images of a mouse treated with the P2X7R radiotracer ^{18}F -JNJ-64413739. PET images were generated by summation of the whole scan (0–30 min) and color-coded to the range of standardized uptake values. (C) Graphs showing P2X7R radiotracer ^{18}F -JNJ-64413739 uptake in different brain regions in control wild-type (wt) mice ($n = 15$; one-way analysis of variance [ANOVA] parametric statistics with post hoc Fisher test). (D) P2X7R radiotracer uptake in the different brain regions analyzed (whole brain, cerebellum and ipsilateral cortex, hippocampus, thalamus, and striatum) in wt control mice and wt mice subjected to SE 48 h after intra-amygdala treatment ($n = 15$ control and $n = 20$ SE); unpaired Student t test). (E) Graphs showing higher P2X7R radiotracer uptake in mice with severe SE (Racine score > 3.5) when compared to mice with mild SE (Racine score ≤ 3.5) 48 h after intra-amygdala KA treatment across all brain regions analyzed (whole brain, cerebellum and ipsilateral cortex, hippocampus, thalamus, and striatum; $n = 15$ control, $n = 14$ mild SE; $n = 6$ severe SE; one-way ANOVA parametric statistics with post hoc Fisher test). (F) Graphs showing strong correlation between P2X7R radiotracer uptake and seizure severity during SE ($n = 20$; Spearman correlation coefficient). (G) Top: Representative PET images (clockwise, axial, sagittal, and coronal views) corresponding to selected brain slices, obtained after administration of ^{18}F -JNJ-64413739 in mice with different Racine scores. PET images have been coregistered with a mouse brain atlas for anatomical localization of brain substructures, including cortex (blue lines), hippocampus (white lines), thalamus (red lines), striatum (orange lines), cerebellum (yellow lines), and brain stem (black lines). Bottom: Magnification of axial slices. %I.D., percentage of injected dose; Cb, cerebellum; Ctrl, control; Cx, cortex; Hippo, hippocampus; ipsi, ipsilateral; Str, striatum; Thal, thalamus.

3.2 | P2X7R radiotracer ^{18}F -JNJ-64413739 uptake in heart and liver correlates with severity of SE

To test whether P2X7R radioligand uptake also increases in peripheral organs after IAKA, we next analyzed several organs including the heart, liver, lungs, and kidneys. As expected, radiotracer levels were highest in the liver, which was followed by the kidneys in control mice and mice subjected to SE (Figure S6A,B). As for the brain, P2X7R tracer uptake was similar between control mice and mice subjected to SE (Figure 3A–D). Tracer uptake was, however, higher in the heart (~25%) and liver (~70%) in mice with more severe SE when compared to mice with milder SE. Radiotracer uptake in the heart and liver showed a strong correlation with severity of SE (Figure 3A,B). No correlation between seizure severity during SE and tracer uptake could be observed for the lungs or kidneys (Figure 3C,D).

3.3 | Increased uptake of ^{18}F -JNJ-64413739 in human brain slices from patients with TLE

Finally, we measured P2X7R tracer uptake ex vivo in brain slices from patients with drug-refractory TLE and compared these to brain slices from control. This showed that P2X7R radioligand uptake was roughly doubled in patients with TLE when compared to control (Figure 4), in line with previous reports showing increased P2X7R expression in resected tissue from TLE patients.^{14,16} Interestingly, P2X7R radiotracer uptake was slightly higher in TLE patients with a less severe hippocampal sclerosis (Figure S7). Confirming specificity of P2X7R

radioligands, specific uptake in brain slices from TLE patients was inhibited when incubated in the presence of nonradioactive JNJ-64413739 (Figure 4).

4 | DISCUSSION

Here, we report increased P2X7R radioligand uptake according to the severity of SE in mice in vivo and in resected brain sections from patients with TLE. P2X7R-based PET imaging may, therefore, represent a new diagnostic tool to determine SE-induced pathology and to identify patients with epilepsy.

PET imaging is increasingly recognized as a promising diagnostic tool for brain diseases including epilepsy, with markers against neuroinflammation gaining significant traction.³⁷ The most commonly used are radiotracers against TSPO.²³ TSPO-PET imaging has shown promising results, with TSPO radiotracer uptake correlating with seizure outcome, pharmacoresistance, and behavioral morbidities in mice.³⁸ TSPO radioligand uptake has also been shown to be increased in brain structures of patients with TLE.²² The use of TSPO radioligands has, however, been hampered by the high level of nonspecific binding of some TSPO radioligands and because binding affinities to TSPO may be influenced by a common polymorphism (rs6971) in the *TSPO* gene, which would require genotyping of patients before conclusive results could be drawn.³⁹ Although TSPO and P2X7R radioligands probably have a similar potential as biomarkers of epilepsy, the most likely advantage of P2X7R radioligands when compared to TSPO radioligands is their potential use as mechanistic biomarkers. P2X7R antagonism has been shown to modulate acute seizures and suppress epileptic seizures.⁵ Moreover, a

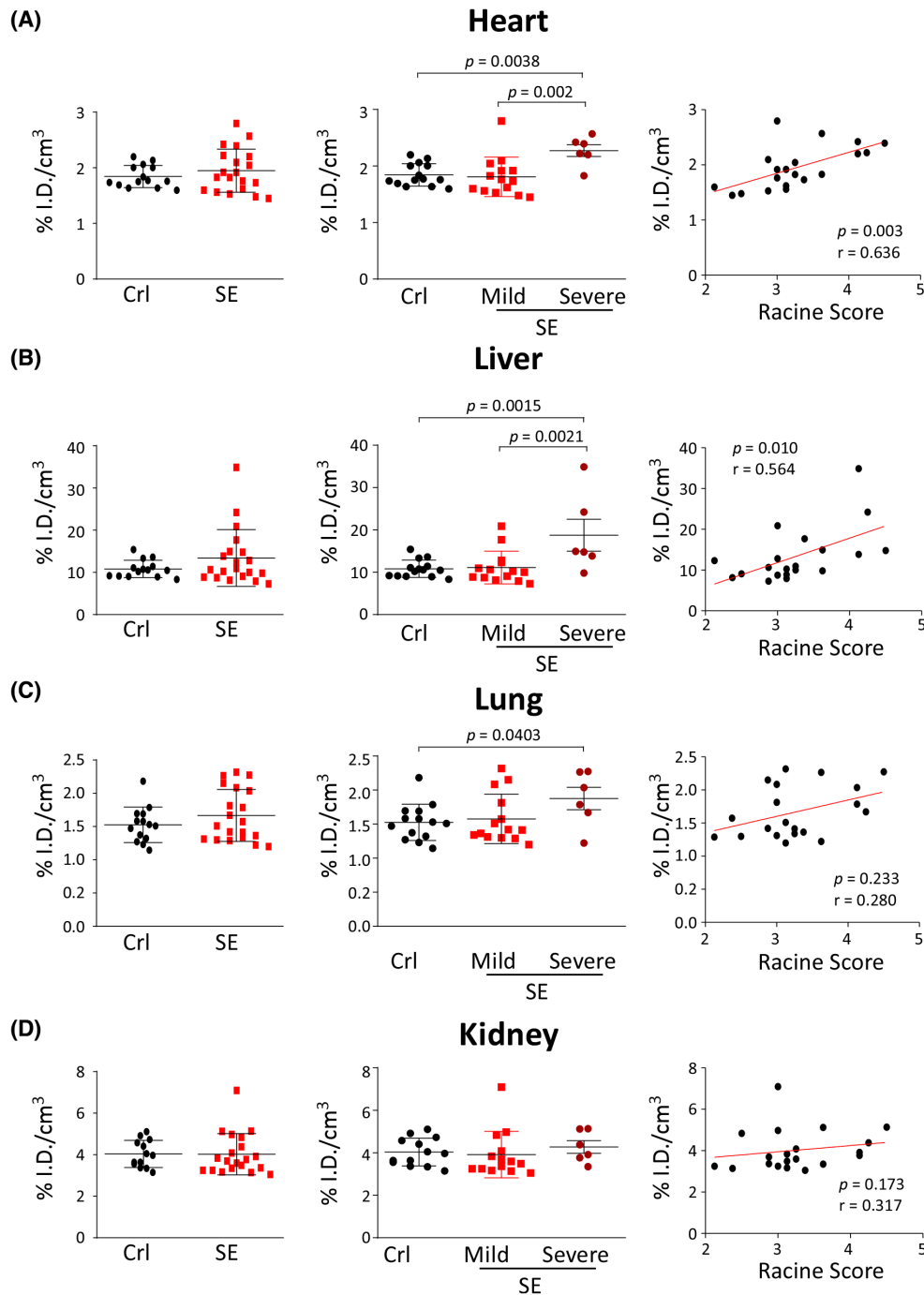


FIGURE 3 P2X7 receptor (P2X7R) radiotracer uptake in peripheral organs after status epilepticus (SE). Graphs show P2X7R radiotracer uptake in different peripheral organs including (A) heart, (B) liver, (C) lung, and (D) kidney 48 h after intra-amygdala kainic acid treatment in control (CrI) mice ($n = 15$) and mice subjected to SE ($n = 20$), including mild SE ($n = 14$) and severe SE ($n = 6$; unpaired Student *t* test for comparison with two groups and one-way analysis of variance parametric statistics with post hoc Fisher test for comparison between three groups; $n = 20$ for correlation between P2X7R radiotracer uptake and seizure severity during SE; Spearman correlation coefficient). %I.D., percentage of injected dose.

recent study by us has shown that increased P2X7R expression leads to unresponsiveness to commonly used ASDs in the clinic.²⁰ Therefore, P2X7R-PET imaging may be a useful tool to identify patients at risk of developing drug-refractory epilepsy and patients who may benefit from P2X7R-based treatments.

One of the main findings of our study is that elevated P2X7R radiotracer uptake is only evident in mice undergoing severe SE, in line with a study showing increased TSPO in mice with severe SE.⁴⁰ Although our study does not show whether P2X7R expression correlates with the severity of epileptogenesis, it is tempting to speculate

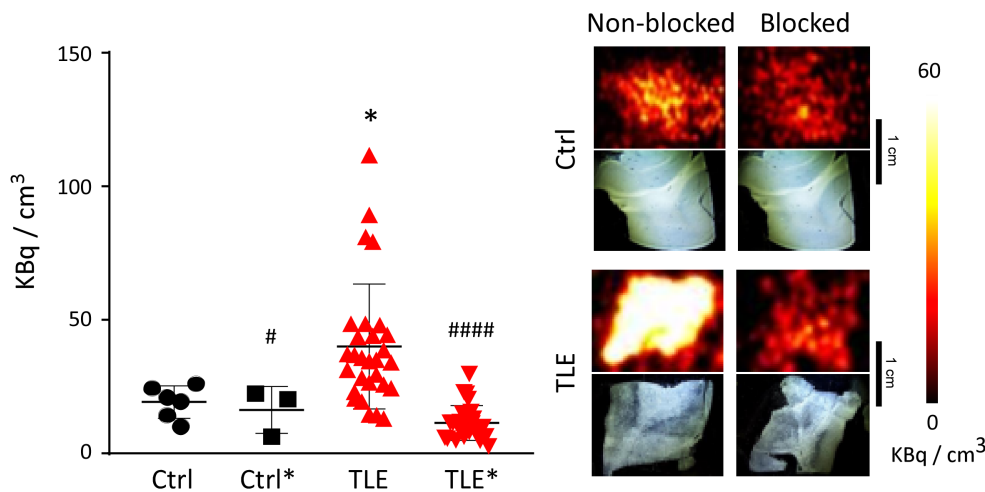


FIGURE 4 Increased P2X7 receptor radiotracer uptake in brain slices from patients with temporal lobe epilepsy (TLE). Graphs and corresponding representative images show radiotracer uptake in resected tissue from patients with TLE and control postmortem tissue slices. Nonblocked (control [Ctrl] and TLE in graphs, “Non-blocked” in the images) and blocked (Ctrl* and TLE* in graphs, “Blocked” in the images) images were obtained by positron emission tomography (PET) of tissue slices after incubation with ^{18}F -JNJ-64413739 (nonblocked) and ^{18}F -JNJ-64413739 with nonradioactive JNJ-64413739 (blocked) to cancel specific binding. Representative photographs of the tissue samples are included below PET images (for the control group, images correspond to two consecutive slices). Ctrl: six brain slices from three controls; Ctrl*: three brain slices from three controls; TLE: 29 brain slices from 14 patients with TLE; TLE*: 26 brain slices from 14 TLE patients. Two-way analysis of variance statistics with multiple comparison are shown. * $p < .05$ represents differences versus ctrl; # $p < .05$ and #### $p < .0001$ represent differences versus TLE. Adjusted p -values: Ctrl versus TLE: .0086; TLE versus ctrl*: .0210; TLE versus TLE*: <.0001.

that a continued increase in P2X7R expression during the seizure-free latent period indicates a more severe disease progression. SE severity has been shown to correlate with the ensuing neurodegeneration and with a more severe epileptic phenotype.^{41–43} Whether P2X7R-PET can be used to identify an epileptic focus remains to be determined. P2X7R expression has, however, been shown to be upregulated throughout the brain including both ipsi- and contralateral brain structures post-SE and during epilepsy,³⁶ in line with our PET studies showing increased P2X7R-PET in several brain regions. This would suggest P2X7R-based PET to be a poor indicator of the epileptic focus. It is, however, important to point out that we have analyzed mice at a single time point (48 h post-SE). Therefore, more specific changes within the epileptic focus may occur at later time points in the model and should be investigated in future studies. However, increased P2X7R expression may support the stratification of patients according to underlying pathology as suggested by our results showing higher radioligand uptake in the brains of mice that experienced more severe SE.

We also show P2X7R radioligand uptake to be increased in peripheral organs, in particular in the heart and the liver. Epilepsy is also characterized by an increased systemic inflammation,⁴⁴ possibly leading to comorbidities that involve peripheral organs such as the heart or the gastrointestinal system. P2X7Rs are, however, also highly expressed in blood cells including lymphocytes,

macrophages, and monocytes,⁴⁵ and we have shown increased P2X7R levels in the blood post-SE in mice and in plasma during epilepsy in patients.⁴⁶ Therefore, although we could speculate that SE leads to increases of P2X7R in the organs themselves, possibly representing an increased inflammatory tissue tone, P2X7R increases in blood may also contribute to the increased P2X7R radioligand uptakes observed peripherally.

Possible confounders include the disruption of the blood–brain barrier (BBB), with both SE and epilepsy reported to lead to the opening of the BBB.⁴⁷ BBB opening may cause tracer perfusion differences that may lead to differences in tracer influx and efflux. We have, however, obtained similar results when using Western blot, showing a strong correlation of P2X7R expression with seizure severity during SE. Nevertheless, future studies should be designed to evaluate the impact of the BBB on tracer uptake post-SE. SE-induced neurodegeneration may constitute another confounding factor. We observed, however, similar increases and correlations for both ipsilateral and nondamaged contralateral brain structures, suggesting P2X7R radioligand uptake is independent on neurodegenerative processes. Moreover, several loss-of-function variants have been identified for P2X7R, and changes in the expression for these during disease progression may impact on P2X7R radiotracer uptake.⁴⁸ Although our results provide the proof of concept of the diagnostic potential of P2X7R-based

radioligands for SE and epilepsy, these results should be validated in other models (e.g., pilocarpine model of SE, TBI-induced epilepsy^{49,50}) and in female mice in the future. Future studies should also be designed to evaluate P2X7R tracer uptake at serial time points from the same animal. Our studies using human tissue suggest P2X7R expression is increased in resected brain tissue from TLE patients, in line with previous data showing increased P2X7R expression in resected patient tissue.^{14,16} Why P2X7R radioligand uptake was higher in patients with less severe hippocampal sclerosis remains to be determined. Differences in cell type expression may be one of the reasons (e.g., astrocytes/microglia vs. neurons). However, these results must be confirmed in much larger patient cohorts. Although we cannot rule out postmortem effects on P2X7R expression, previous studies have shown no impact on P2X7R expression during simulated postmortem experiments in mice.¹⁶ Finally, although we assume that changes in P2X7R expression are due to inflammatory processes triggered by SE and epilepsy, this will need to be further investigated in future studies (e.g., cell type-specific P2X7R knockout mice).

In summary, our study provides the first evidence of the diagnostic potential of P2X7R-based PET imaging for seizure-induced pathology and epilepsy. Importantly, with the demonstrated role for P2X7R during seizures and epilepsy,³ P2X7R-based PET may represent a promising tool to identify patients at risk of epilepsy, and to identify patients who would benefit from P2X7R-based treatments.

AUTHOR CONTRIBUTIONS

Conceptualization and methodology: Vanessa Gómez-Vallejo, Jordi Llop, and Tobias Engel. Validation, formal analysis, investigation, and data curation: James Morgan, Oscar Moreno, Mariana Alves, Zuriñe Baz, Aida Menéndez Méndez, Ciara Melia, Jonathon Smith, Hanna Leister, Jordi Llop, and Tobias Engel. Resources: Annette Nicke, Marc Ceusters, Anindya Bhattacharya, David C. Henshall, Vanessa Gómez-Vallejo, Jordi Llop, and Tobias Engel. Writing—original draft preparation: Jordi Llop and Tobias Engel. Writing—review and editing: David C. Henshall, Jordi Llop, and Tobias Engel. Preparation of figures: James Morgan, Mariana Alves, Ciara Melia, Jordi Llop, and Tobias Engel. Project administration: Jordi Llop and Tobias Engel. Funding acquisition: David C. Henshall, Jordi Llop, Annette Nicke, and Tobias Engel. All authors reviewed the manuscript.

ACKNOWLEDGMENTS

This work was supported by funding from Science Foundation Ireland (17/CDA/4708, and cofunded under the European Regional Development Fund and by FutureNeuro industry partners 16/RC/3948), the

European Union's Horizon 2020 research and innovation program under the Marie Skłodowska-Curie grant agreement (766124), the H2020 Marie Skłodowska-Curie Actions Individual Fellowship (884956), the Irish Research Council (Government of Ireland Postdoctoral Fellowship Programme, GOIPD/2020/865), and the German Research Foundation (project ID: 335447717–SFB 1328 (A15 to A.N.)). Part of the imaging work was funded by MCIN/AEI/10.13039/501100011033 (PID2020-117656RB-I00 and MDM-2017-0720). We thank Friedrich Koch-Nolte for providing the P2X7R-specific nanobody. We would also like to thank the UK Brain Bank for providing human brain tissue. Open access funding provided by IReL.

CONFLICT OF INTEREST

A.B. is and M.C. was employed by Janssen Research and Development. None of the other authors has any conflict of interest to disclose.

ORCID

James Morgan  <https://orcid.org/0000-0002-7833-3863>

David C. Henshall  <https://orcid.org/0000-0001-6237-9632>

Jordi Llop  <https://orcid.org/0000-0002-0821-9838>

Tobias Engel  <https://orcid.org/0000-0001-9137-0637>

REFERENCES

- Engel J Jr, Pitkanen A. Biomarkers for epileptogenesis and its treatment. *Neuropharmacology*. 2020;167:107735.
- Pitkanen A, Nehlig A, Brooks-Kayal AR, et al. Issues related to development of antiepileptogenic therapies. *Epilepsia*. 2013;54(Suppl 4):35–43.
- Beamer E, Kuchukulla M, Boison D, Engel T. ATP and adenosine-two players in the control of seizures and epilepsy development. *Prog Neurobiol*. 2021;204:102105.
- Burnstock G. Introduction to purinergic Signalling in the brain. *Adv Exp Med Biol*. 2020;1202:1–12.
- Beamer E, Fischer W, Engel T. The ATP-gated P2X7 receptor As a target for the treatment of drug-resistant epilepsy. *Front Neurosci*. 2017;11:21.
- Surprenant A, Rassendren F, Kawashima E, North RA, Buell G. The cytolytic P2Z receptor for extracellular ATP identified as a P2X receptor (P2X7). *Science*. 1996;272(5262):735–8.
- Monif M, Reid CA, Powell KL, Smart ML, Williams DA. The P2X7 receptor drives microglial activation and proliferation: a trophic role for P2X7R pore. *J Neurosci*. 2009;29(12):3781–91.
- Di Virgilio F, Dal Ben D, Sarti AC, Giuliani AL, Falzoni S. The P2X7 receptor in infection and inflammation. *Immunity*. 2017;47(1):15–31.
- Sperlagh B, Illes P. P2X7 receptor: an emerging target in central nervous system diseases. *Trends Pharmacol Sci*. 2014;35(10):537–47.
- Jimenez-Mateos EM, Smith J, Nicke A, Engel T. Regulation of P2X7 receptor expression and function in the brain. *Brain Res Bull*. 2019;151:153–63.

11. Vianna EP, Ferreira AT, Naffah-Mazzacoratti MG, et al. Evidence that ATP participates in the pathophysiology of pilocarpine-induced temporal lobe epilepsy: fluorimetric, immunohistochemical, and Western blot studies. *Epilepsia*. 2002;43(Suppl 5):227–9.
12. Dona F, Ulrich H, Persike DS, et al. Alteration of purinergic P2X4 and P2X7 receptor expression in rats with temporal-lobe epilepsy induced by pilocarpine. *Epilepsy Res*. 2009;83(2–3):157–67.
13. Engel T, Gomez-Villafuertes R, Tanaka K, Mesuret G, Sanz-Rodriguez A, Garcia-Huerta P, et al. Seizure suppression and neuroprotection by targeting the purinergic P2X7 receptor during status epilepticus in mice. *FASEB J*. 2012;26(4):1616–28.
14. Jimenez-Pacheco A, Mesuret G, Sanz-Rodriguez A, Tanaka K, Mooney C, Conroy R, et al. Increased neocortical expression of the P2X7 receptor after status epilepticus and anticonvulsant effect of P2X7 receptor antagonist A-438079. *Epilepsia*. 2013;54(9):1551–61.
15. Jimenez-Mateos EM, Arribas-Blazquez M, Sanz-Rodriguez A, Concannon C, Olivos-Ore LA, Reschke CR, et al. microRNA targeting of the P2X7 purinoceptor opposes a contralateral epileptogenic focus in the hippocampus. *Sci Rep*. 2015;5:17486.
16. Jimenez-Pacheco A, Diaz-Hernandez M, Arribas-Blazquez M, et al. Transient P2X7 receptor antagonism produces lasting reductions in spontaneous seizures and gliosis in experimental temporal lobe epilepsy. *J Neurosci*. 2016;36(22):5920–32.
17. Kim JE, Kang TC. The P2X7 receptor-pannexin-1 complex decreases muscarinic acetylcholine receptor-mediated seizure susceptibility in mice. *J Clin Invest*. 2011;121(5):2037–47.
18. Rozmer K, Gao P, Araujo MGL, et al. Pilocarpine-induced status epilepticus increases the sensitivity of P2X7 and P2Y1 receptors to nucleotides at neural progenitor cells of the juvenile rodent hippocampus. *Cereb Cortex*. 2017;27(7):3568–85.
19. Amhaoul H, Ali I, Mola M, van Eetveldt A, Szewczyk K, Missault S, et al. P2X7 receptor antagonism reduces the severity of spontaneous seizures in a chronic model of temporal lobe epilepsy. *Neuropharmacology*. 2016;105:175–85.
20. Beamer E, Morgan J, Alves M, et al. Increased expression of the ATP-gated P2X7 receptor reduces responsiveness to anti-convulsants during status epilepticus in mice. *British Journal of Pharmacology*. 2022;179(12):2986–3006.
21. Amhaoul H, Hamaide J, Bertoglio D, Reichel SN, Verhaeghe J, Geerts E, et al. Brain inflammation in a chronic epilepsy model: evolving pattern of the translocator protein during epileptogenesis. *Neurobiol Dis*. 2015;82:526–39.
22. Gershen LD, Zanotti-Fregonara P, Dustin IH, Liow JS, Hirvonen J, Kreisl WC, et al. Neuroinflammation in temporal lobe epilepsy measured using positron emission tomographic imaging of translocator protein. *JAMA Neurol*. 2015;72(8):882–8.
23. Koeppe MJ, Arstad E, Bankstahl JP, et al. Neuroinflammation imaging markers for epileptogenesis. *Epilepsia*. 2017;58(Suppl 3):11–9.
24. Wolf BJ, Brackhan M, Bascunana P, et al. TSPO PET identifies different anti-inflammatory minocycline treatment response in two rodent models of Epileptogenesis. *Neurotherapeutics*. 2020;17(3):1228–38.
25. Berdyeva T, Xia C, Taylor N, He Y, Chen G, Huang C, et al. PET imaging of the P2X7 Ion Channel with a novel tracer [(18)F]JNJ-64413739 in a rat model of Neuroinflammation. *Mol Imaging Biol*. 2019;21(5):871–8.
26. Kolb HC, Barret O, Bhattacharya A, Chen G, Constantinescu C, Huang C, et al. Preclinical evaluation and nonhuman primate receptor occupancy study of (18)F-JNJ-64413739, a PET Radioligand for P2X7 receptors. *J Nucl Med*. 2019;60(8):1154–9.
27. Mouri G, Jimenez-Mateos E, Engel T, Dunleavy M, Hatazaki S, Paucard A, et al. Unilateral hippocampal CA3-predominant damage and short latency epileptogenesis after intra-amygdala microinjection of kainic acid in mice. *Brain Res*. 2008;1213:140–51.
28. Kaczmarek-Hajek K, Zhang J, Kopp R, et al. Re-evaluation of neuronal P2X7 expression using novel mouse models and a P2X7-specific nanobody. *Elife*. 2018;7:e36217.
29. Jimenez-Mateos EM, Engel T, Merino-Serrais P, McKiernan RC, Tanaka K, Mouri G, et al. Silencing microRNA-134 produces neuroprotective and prolonged seizure-suppressive effects. *Nat Med*. 2012;18(7):1087–94.
30. Engel T, Gomez-Sintes R, Alves M, et al. Bi-directional genetic modulation of GSK-3beta exacerbates hippocampal neuropathology in experimental status epilepticus. *Cell Death Dis*. 2018;9(10):969.
31. Miller-Delaney SF, Bryan K, Das S, et al. Differential DNA methylation profiles of coding and non-coding genes define hippocampal sclerosis in human temporal lobe epilepsy. *Brain*. 2015;138(Pt 3):616–31.
32. Koole M, Schmidt ME, Hijzen A, Ravenstijn P, Vandermeulen C, van Weehaeghe D, et al. (18)F-JNJ-64413739, a novel PET ligand for the P2X7 Ion Channel: radiation dosimetry, kinetic modeling, test-retest variability, and occupancy of the P2X7 antagonist JNJ-54175446. *J Nucl Med*. 2019;60(5):683–90.
33. Mertens N, Schmidt ME, Hijzen A, van Weehaeghe D, Ravenstijn P, Depre M, et al. Minimally invasive quantification of cerebral P2X7R occupancy using dynamic [(18)F]JNJ-64413739 PET and MRA-driven image derived input function. *Sci Rep*. 2021;11(1):16172.
34. Ory D, Celen S, Gijsbers R, van Den Haute C, Postnov A, Koole M, et al. Preclinical evaluation of a P2X7 receptor-selective radiotracer: PET studies in a rat model with local overexpression of the human P2X7 receptor and in nonhuman primates. *J Nucl Med*. 2016;57(9):1436–41.
35. Ulmann L, Levavasseur F, Avignone E, Peyrourou R, Hirbec H, Audinat E, et al. Involvement of P2X4 receptors in hippocampal microglial activation after status epilepticus. *Glia*. 2013;61(8):1306–19.
36. Morgan J, Alves M, Conte G, Menéndez-Méndez A, de Diego-Garcia L, de Leo G, et al. Characterization of the expression of the ATP-gated P2X7 receptor following status epilepticus and during epilepsy using a P2X7-EGFP reporter mouse. *Neurosci Bull*. 2020;36(11):1242–58.
37. Meyer JH, Cervenka S, Kim MJ, Kreisl WC, Henter ID, Innis RB. Neuroinflammation in psychiatric disorders: PET imaging and promising new targets. *Lancet Psychiatry*. 2020;7(12):1064–74.
38. Bouilleret V, Dedeurwaerdere S. What value can TSPO PET bring for epilepsy treatment? *Eur J Nucl Med Mol Imaging*. 2021;49(1):221–33.
39. Scott G, Mahmud M, Owen DR, Johnson MR. Microglial positron emission tomography (PET) imaging in epilepsy: applications, opportunities and pitfalls. *Seizure*. 2017;44:42–7.

40. Dedeurwaerdere S, Callaghan PD, Pham T, Rahardjo GL, Amhaoul H, Berghofer P, et al. PET imaging of brain inflammation during early epileptogenesis in a rat model of temporal lobe epilepsy. *EJNMMI Res.* 2012;2(1):60.
41. Klitgaard H, Matagne A, Vanneste-Goemaere J, Margineanu DG. Pilocarpine-induced epileptogenesis in the rat: impact of initial duration of status epilepticus on electrophysiological and neuropathological alterations. *Epilepsy Res.* 2002;51(1–2):93–107.
42. Santamarina E, Gonzalez M, Toledo M, Sueiras M, Guzman L, Rodriguez N, et al. Prognosis of status epilepticus (SE): relationship between SE duration and subsequent development of epilepsy. *Epilepsy Behav.* 2015;49:138–40.
43. Sharma S, Puttachary S, Thippeswamy A, Kanthasamy AG, Thippeswamy T. Status epilepticus: behavioral and electroencephalography seizure correlates in Kainate experimental models. *Front Neurol.* 2018;9:7.
44. Rana A, Musto AE. The role of inflammation in the development of epilepsy. *J Neuroinflammation.* 2018;15(1):144.
45. Savio LEB, de Andrade MP, da Silva CG, Coutinho-Silva R. The P2X7 receptor in inflammatory diseases: angel or demon? *Front Pharmacol.* 2018;9:52.
46. Conte G, Menendez-Mendez A, Bauer S, et al. Circulating P2X7 receptor signaling components as diagnostic biomarkers for temporal lobe epilepsy. *Cell.* 2021;10(9):2444.
47. Marchi N, Granata T, Ghosh C, Janigro D. Blood-brain barrier dysfunction and epilepsy: pathophysiologic role and therapeutic approaches. *Epilepsia.* 2012;53(11):1877–86.
48. Van Weehaeghe D, Koole M, Schmidt ME, et al. [¹¹C] JNJ54173717, a novel P2X7 receptor radioligand as marker for neuroinflammation: human biodistribution, dosimetry, brain kinetic modelling and quantification of brain P2X7 receptors in patients with Parkinson's disease and healthy volunteers. *Eur J Nucl Med Mol Imaging.* 2019;46(10):2051–64.
49. Brackhan M, Bascunana P, Postema JM, et al. Serial quantitative TSPO-targeted PET reveals peak microglial activation up to 2 weeks after an epileptogenic brain insult. *J Nucl Med.* 2016;57(8):1302–8.
50. Dulla CG, Pitkanen A. Novel approaches to prevent Epileptogenesis after traumatic brain injury. *Neurotherapeutics.* 2021;18(3):1582–601.

SUPPORTING INFORMATION

Additional supporting information can be found online in the Supporting Information section at the end of this article.

How to cite this article: Morgan J, Moreno O, Alves M, Baz Z, Menéndez Méndez A, Leister H, et al. Increased uptake of the P2X7 receptor radiotracer ¹⁸F-JNJ-64413739 in the brain and peripheral organs according to the severity of status epilepticus in male mice. *Epilepsia.* 2023;64:511–523. <https://doi.org/10.1111/epi.17484>